

**PRECIPITATION MEASUREMENT USING SIR-C
A FEASIBILITY STUDY**

Atiq Ahamad and Richard K. Moore

Radar Systems and Remote Sensing Laboratory
Department of Electrical Engineering and Computer Science, University of Kansas
2291 Irving Hill Road, Lawrence, Kansas 66045-2969
TEL: 913/864-4835 * FAX: 913/864-7789 * OMNET: KANSAS.U.RSL

RSL Technical Report 8370-1

November 1993

Sponsored by:

NASA Jet Propulsion Laboratory
Pasadena CA 91109

Grant NAS7-918, 958522

ABSTRACT

A precipitation detection and measurement experiment is planned for the SIR-C /X-SAR mission. This study was conducted to determine under what conditions an off-nadir experiment is feasible. We investigated the signal-to-clutter ratio, the signal-to-noise ratio, and the minimum detectable rain rate. Available models, used in previous studies, were used for the surface clutter and the rain echo. The study also considers the attenuation of the returns at X band. We conclude that an off-nadir rain-measurement experiment is feasible only for rain rates > 10 mm/hr for look angles $> 60^\circ$. For the range of look angles $5^\circ < \theta_l < 50^\circ$, the rain rate required is very high for adequate signal-to-clutter ratio, and hence the feasibility of the experiment.

1.0 INTRODUCTION

The detection and measurement of precipitation from space platforms will be important in a wide spectrum of meteorological problems. A precipitation detection and measurement experiment was accepted for the SIR-C/X-SAR mission. Although climatological applications require observing the rainfall over a long period of time, the results obtained from this proof-of-concept experiment will help demonstrate synthetic-aperture radar (SAR) capabilities for short-term rain measurement and allow partial verification of the rain-retrieval algorithm. The results may also be useful for meteorological research, but this is doubtful in view of the limited time for the experiment.

We expect that the SIR-C /X-SAR sensors can measure rain quantitatively for moderate to intense rain rates (> 10 mm/hr), at high off-vertical angles. It is proposed, if possible, to compare the observed SIR-C /X-SAR radar backscatter power with in situ data from calibrated ground-based radars.

Rain-rate estimation from backscatter signal strength is the simplest method for precipitation detection. However, the backscatter method can underestimate the true rain rate (Goldhirsh 1988) when used without correcting for attenuation. Since the X-SAR operates at 9.7 GHz, where attenuation can cause problems, correction factors are necessary.

The report outlines a study to determine the feasibility of rain retrieval using the X-SAR at off-vertical angles of incidence. The lower magnitude of backscatter at C band makes this frequency impractical.

2.0 GEOMETRY

For vertical incidence and a narrow transmitted pulse, the backscattered power from the hydrometeors arrives at the receiver prior to the large surface contribution. At non-vertical

viewing angles, however, the surface return arrives simultaneously with the desired echo (see Fig. 1a). Thus, the surface clutter can mask the returns due to the rain at the surface.

The geometry shown in Fig. 1b is for non-vertical viewing angles making the plane-earth assumption. From elementary geometry we can compute the dimensions of the observed volume as a function of the look angle. The beam below the cloud top is divided into range cells corresponding to a slant-range resolution of 15 m. The swath R_s on the ground for vertical beamwidth β_v and satellite height h is

$$R_s = h [\tan(\theta_1) - \tan(\theta)] \quad (1)$$

where

$$\theta_1 = \beta_v + \theta \quad (2)$$

and

$$R_{s1} = (h - h_1) [\tan(\theta_1) - \tan(\theta)] \quad (3)$$

is the swath width at the cloud top, and h_1 is the thickness of the rain. Computation of the swath gives us an idea of the coverage possible by the X-SAR mission.

The number of rain-filled cells is

$$n = \frac{R_{1\max}}{r_R} \quad (4)$$

where

$$R_{1\max} = \frac{h_1}{\cos(\theta_1)} \quad (5)$$

is the range in the rain-filled volume and r_R is the range resolution. Here we use a simple model that ignores the main beam shape and the sidelobes, since we need a general forecast of

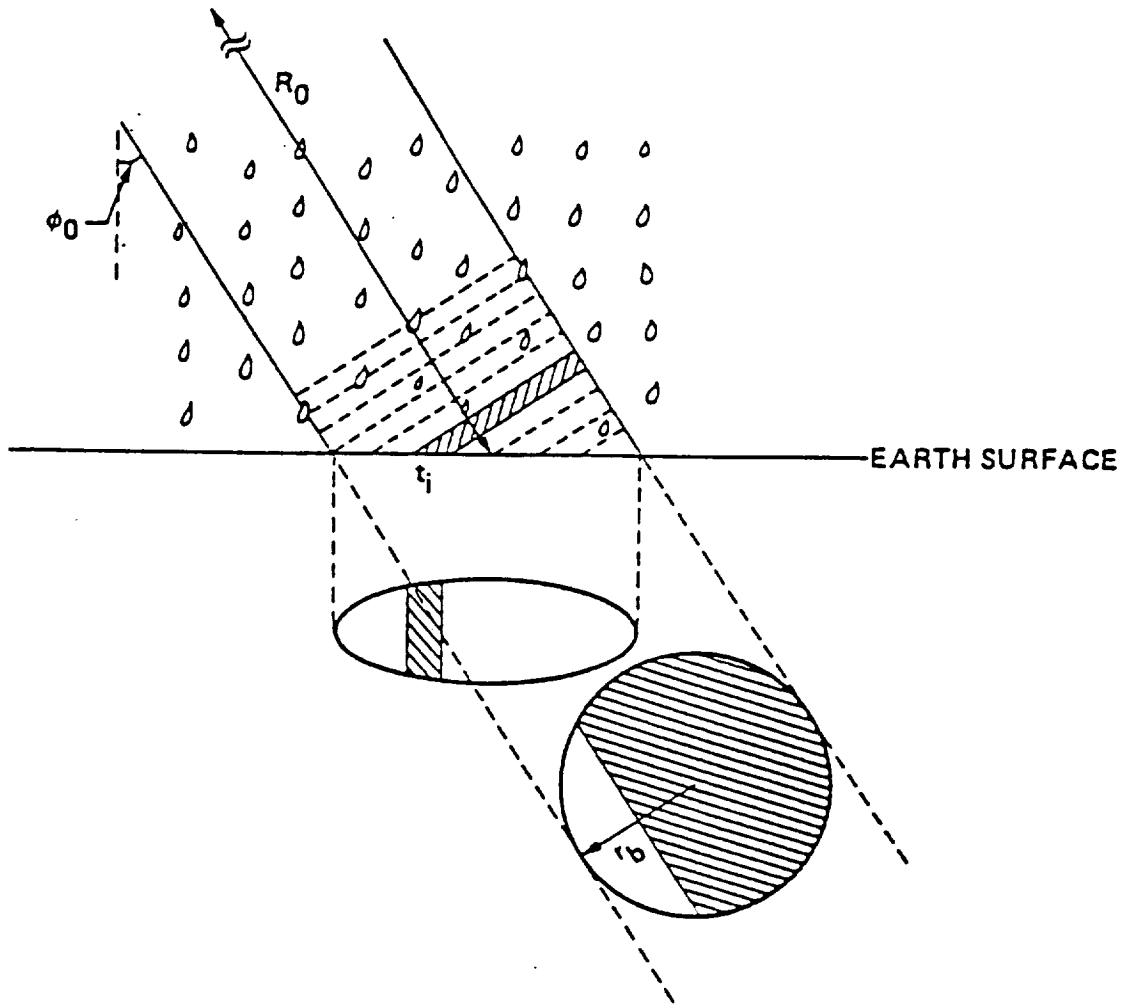


Fig.1a Geometry with ideal circular aperture showing the rain cell and the corresponding ground area coupled to it (Im and Atlas, 1987).

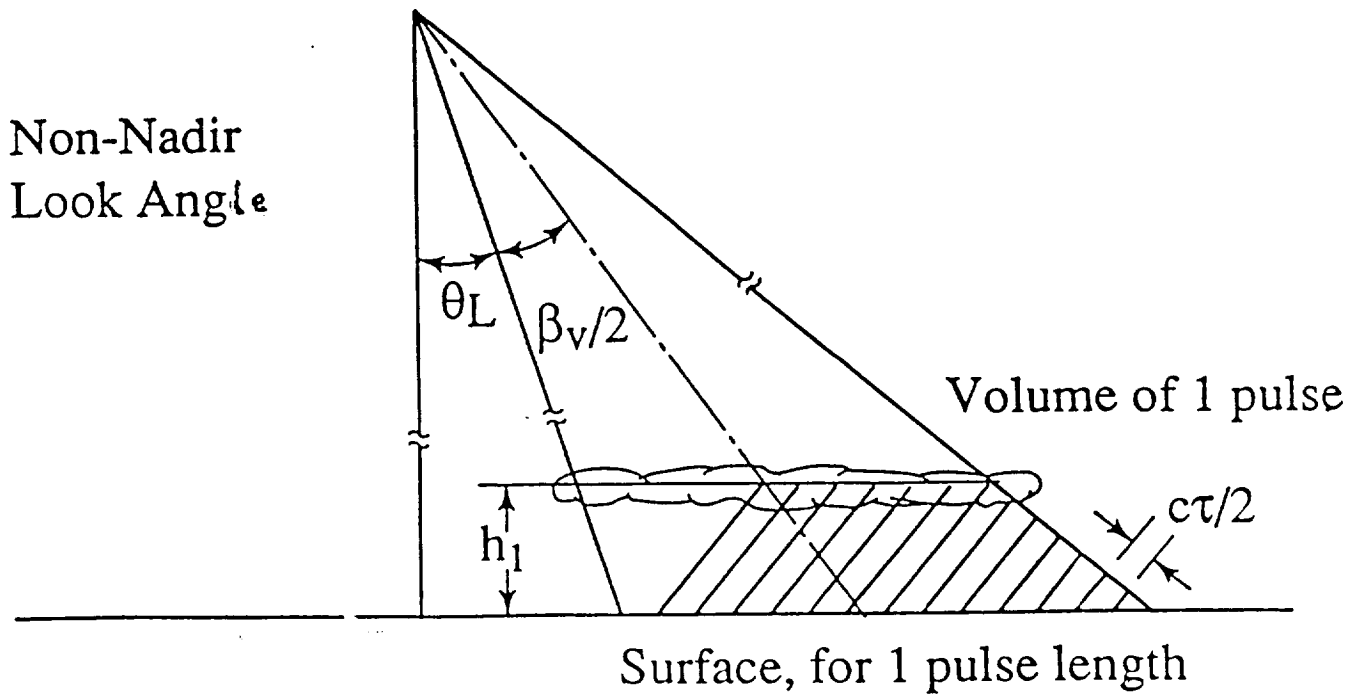


Fig.1b Geometry for non vertical viewing angles.

performance. Fig. 2 shows three cases of cell lengths.

Region 1. Pulse position at the end of the return that extends up to the edge of the beam, not to the rain top.

Region 2. Pulse position in the center of the return that extends from the ground to the rain top.

Region 3. Pulse position at the start of the return that extend from the inner edge of the beam to the cloud top and includes no ground return.

If we assume that the rain extends throughout the swath, most of the returns correspond to those in Region 2. Further, since we can calculate the signal-to-noise ratio and the signal-to-clutter ratio using the real-aperture parameters, the width of the cell in the direction normal to the plane of the paper is

$$r_{an} = \beta_a [R - nr_R] \quad (6)$$

where β_a is the azimuth beamwidth, R is the slant range to the ground, r_R is the range resolution and n is the cell number, measured from maximum R backward.

2.1 CELL VOLUME CALCULATIONS

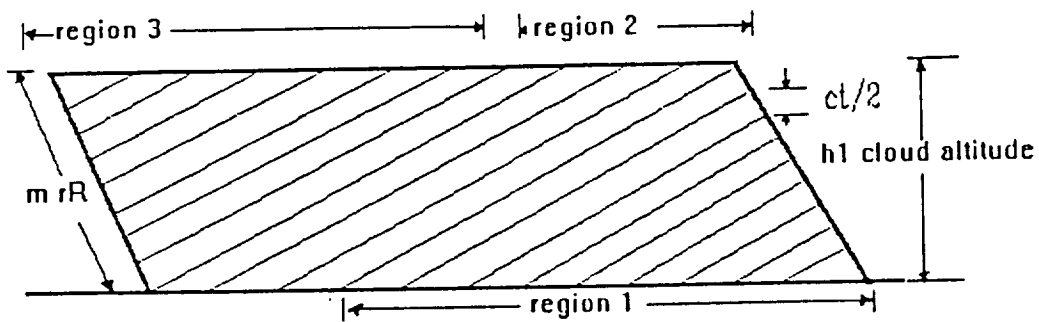
In region 1 (longest range) the volume of the n^{th} cell from the bottom is

$$V_n = L r_R r_a \quad (7)$$

where

$$L = n r_R \cot(\theta_{av}) \quad (8)$$

is the length of the rain cell in the plane of incidence and normal to the ray from the radar to the rain. The width of the rain cell in the direction normal to the plane of the paper is r_a , r_R is the slant-range resolution and θ_{av} is the average angle of incidence.



off nadir geometry illustrating the three regions of interest

Fig.2 Off vertical geometry exploded to show the region of interest.

In region 2 (center of the beam) the volume is the same for all pulses.

$$V_n = r_a r_R \frac{h_1}{\sin(\theta_{av})} \quad (9)$$

Here θ_{av} , the average angle of incidence, is used when calculating the range to the pulse volume (bounded by concentric spheres) to avoid the complication arising because it varies slightly as move toward the outer edge. The ground area coupled to the rain cell in the above two cases is

$$A = r_R \left(\frac{r_a}{\sin(\theta_r)} \right) \quad (10)$$

where θ_r is θ_1 in region 1 and θ_{av} in region 2.

In region 3 (shortest range) there is no ground return. The length of the cell, however, is

$$L = m R_r \cot(\theta) \quad (11)$$

where m is the index starting from the top. Even if the rain cell fails to fill the swath completely three similar regions may be identified, but the number of constant volume rain cells is less, as seen from Fig. 3.

Region 1 The region for which returns come from the far edge of the rain cell.

Region 2 The region for which returns come from near the center of the cell.

Region 3 The region for which returns come from near the edge of the cell.

The volume of the rain cells at the center is the same as that in region 2 of the completely filled beam. However, for region 1, if

$$h_n = n \left(\frac{r_R}{\cos(\theta_{av})} \right), \quad (12)$$

and the length of the cell is

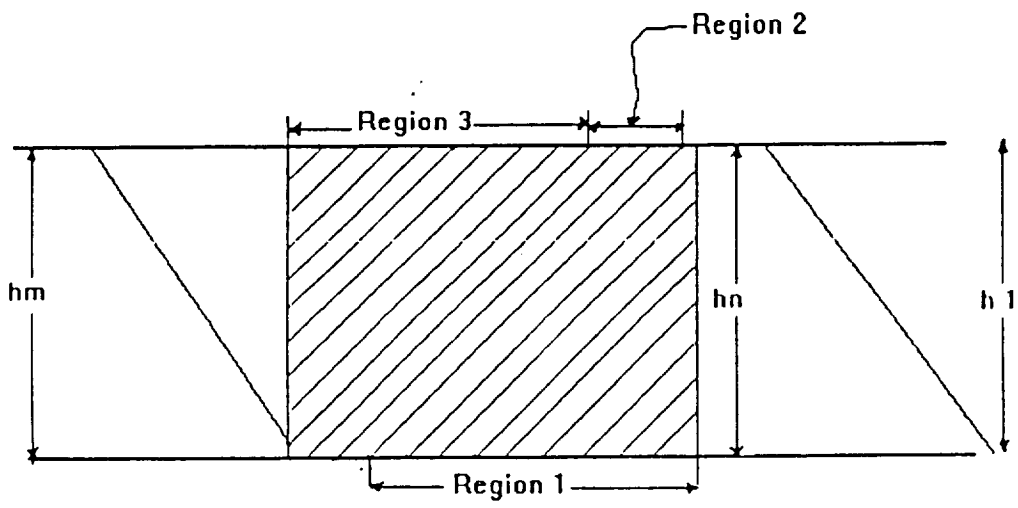


Fig.3 Geometry of Fig.2 modified when rain partially fills the beam.

$$L = \frac{h_n}{\sin(\theta_{av})} \quad (13)$$

and the volume of the cell can be written as

$$V_n = r_R^2 r_a \left(\frac{n}{\cos(\theta_{av}) \sin(\theta_{av})} \right) \quad (14)$$

where n is an integer and h_n is defined as the distance to the pulse intersection with the outer edge of the cell.

In region 3

$$h_m = m \left(\frac{r_R}{\cos(\theta_{av})} \right) \quad (15)$$

where m is an integer value corresponding to the cell number (starting from the top) and h_m is the height to the intersection of the range cell with the inner edge of the rain cell.

The length of the cell from this point to the top is

$$L = \frac{h_m}{\sin(\theta_{av})} \quad (16)$$

The volume of the rain cell in this region is

$$V_m = r_a r_R \left(\frac{h_m}{\sin(\theta_{av})} \right) \quad (17)$$

which reduces to

$$V_m = m r_a \left(\frac{r_R^2}{\sin(\theta_{av}) \cos(\theta_{av})} \right) \quad (18)$$

Thus the volume of the resolution cell in the rain is a function of the look angle and the range resolution only.

For plane-earth geometry, the look angle and the incidence angle are the same. However, for the spherical Earth they are not. Since the rain height is small compared to the satellite

height, we can use incidence angle in the calculations (i.e., we may use all the equations discussed previously with incidence angles in them).

3.0 SURFACE ECHO MODEL

The circle-flight experiment, developed by Jones et al. (1978) at NASA Langley Research Center, allowed the accurate measurement of azimuth variation of echoes from the sea for the first time. Previous measurements were only for up, down, and cross winds. A basic model function for azimuth variation was developed from the Jones measurement. The resulting equation is

$$\sigma^{\circ} = A + B \cos\phi + C \cos 2\phi \quad (19)$$

Fung and Chan(1977) also use this model, in part because of the Jones result. These measurements were a part of the Advanced Application Flight Experiment (AAFE).

Because of the better calibration of the AAFE Radscat, and because there were large number of flights accompanied by high quality surface observations, this was one of the most reliable aircraft wind response data sets available until recently. Soofi (1978) developed an empirical model to calculate the magnitude of the ocean returns. This model matches closely with the AAFE Radscat, SEASAT and SKYLAB data (Schroeder. L.C et al., 1985). It also accounts for various wind speeds and aspect angles (direction of the wind with respect to the radar bore sight). The equation for this ocean-clutter model is

$$\sigma^{\circ}_{db}(f, \theta, W, \phi) = A + B \cos \phi + C \cos 2\phi \quad (20)$$

where the coefficients A, B and C take values depending on the polarization used.

For the polarization of interest (VV) the values of A, B and C are functions of wind speed, angle of incidence and frequency.

$$\begin{aligned}
A &= (-24.642 + 10.8256 \log W) + (-0.1983 - 0.0017 \log W) \theta \\
&+ (1.1725 - 0.6191 \log W) f + (-0.0123 + 0.0124 \log W) f \theta \\
B &= (0.4337 - 0.7041 \log W) + (-0.0085 + 0.0143 \log W) \theta \\
&+ (-0.0082 + 0.0153 \log W) f + (0.0004 - 0.006 \log W) f \theta \\
C &= (0.1619 + 1.4160 \log W) + (-0.0086 + 0.0089 \log W) \theta \\
&+ (0.0067 - 0.0124 \log^2) f
\end{aligned}$$

Here the frequency is in Ghz, the wind speed in m/s and the angle in degrees. This model predicts the value of the coefficients within about 2 dB of the mean. The maximum error occurs at 4 Ghz.

3.1 EFFECT OF RAIN ON SURFACE RETURN

The modification of the backscatter due to impinging rain drops may be important. In the area of the ocean where it is raining, the cross section increases due to the impinging rain drops. Moore et al. (1979) showed that, for a given wind speed, the backscatter cross section depends on the rain rate, as shown in Fig. 4. Hansen (1986) later conducted both laboratory and field experiments that show a significant enhancement of the echo intensity as a result of the splashes and ripples due to the impinging raindrops. This enhancement of the radar return applies only for low wind speeds. At high wind speeds the effect of rain rate on backscatter modification is lost; i.e., the backscatter at these high wind speeds is independent of the rain rate

(Moore et al., 1979; Blivens and Norcross, 1988) as seen in Fig. 4.

4.0 SIGNAL-TO-CLUTTER RATIO

The backscatter method uses the returned echo from the rain to compute the rain rate. For non-vertical angles of incidence, however, the surface returns arrive simultaneously with the desired echo and increase in magnitude as the range gates within the mainbeam begin to intersect the surface (see Fig. 1a). Thus, the surface clutter can mask the return due to the rain. For the backscatter method to work, the echo from the rain should be substantially above the surface echo to allow separating them. Hence, we compute the **signal-to-clutter ratio** (SCR). This is defined as the ratio of the desired signal (rain return) to the clutter signal (surface return). Since the surface and rain are excited by the power from the same transmitter, one need not use the radar equation in its entirety for these calculations. The scattering coefficient for the rain has the units m^3 but the scattering coefficient of the ground has the units m^2 . To compare the returns, one must multiply the rain returns by the volume of the rain cell and the surface returns by the area of the surface coupled to the corresponding rain cell.

The scattering coefficient for the rain, when λ is in cm, (Ulaby, Moore, and Fung; 1986) is

$$\sigma_v = \frac{\pi^5}{\lambda^4} Z |k|^2 10^{-10} \quad (21)$$

The volume of the rain cell is given by

$$V = r_R r_a L \quad (22)$$

where r_R is the range resolution, r_a , the azimuth resolution and L is the length of the rain cell, discussed in the previous section. Since the scattering coefficient of the ground calculated from

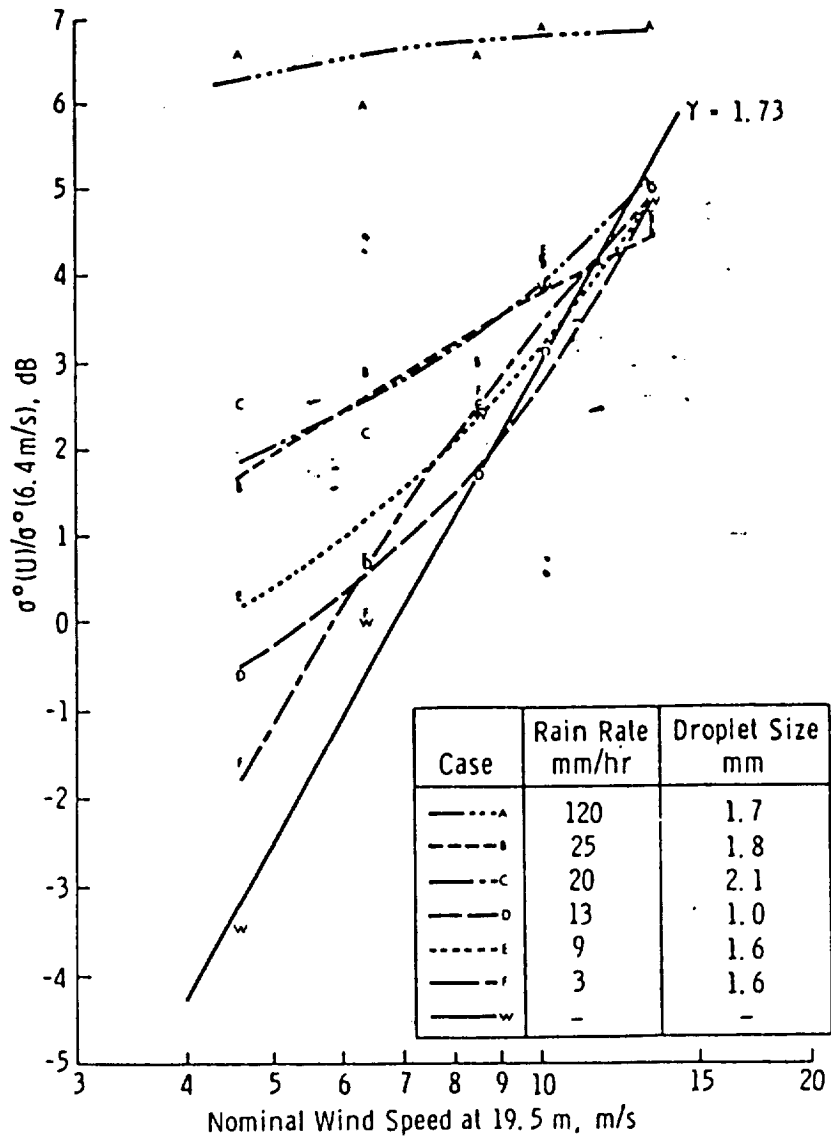


Fig.4 Modification of the ocean backscatter due to impinging rain drops.

the model is in dB, we can get the total cross section by adding $10 \log(\text{ground area})$ to σ_{dB} , obtaining σ_{gdB} as

$$\sigma_{gdB} = \sigma_{dB}^o + 10 \log(r_a R_{s1}) \quad (23)$$

where r_a and R_{s1} are from geometry discussed in the previous section.

To determine how much the rain signal lies above the ground signal we compute

$$\Delta \sigma_{dB} = \sigma_{vl_{dB}} - \sigma_{gdB} \quad (24)$$

where

$$\sigma_{vl_{dB}} = 10 \log(\sigma_r) \quad (25)$$

and

$$\sigma_r = \sigma_v V \quad (26)$$

Now let us introduce the concept of ideal rain cells. An ideal rain cell is defined as a resolution cell that has a completely rain-filled volume. Clearly these are the kind of rain cells that are of interest for our calculations. From the previous discussion it is clear that the rain cells in region 2 come close to our definition of an ideal rain cell.

4.1 SIGNAL-TO-CLUTTER RATIO IN THE MAIN PART OF THE RAIN

Let us now consider a more realistic case, including attenuation effects. For non-vertical look angles, if the entire beam volume is assumed to be rain filled, all the returns from the ground are attenuated. Further, as we move from the top to bottom of a rain cell, the signal is attenuated increasingly as shown in Fig. 5. To consider this type of attenuation for each rain cell, we must determine the attenuation factor for different path lengths. Thus the actual surface echo is

$$\sigma_s = \sigma_o e^{-\alpha \cdot 2 R_{1\max}} A_o \quad (27)$$

where $R_{1\max}$ is the range in the rain. The actual rain echo is given by

$$\sigma_r = r_R r_a L \sigma_v k_{er} \quad (28)$$

where

$$k_{er} = \int_0^{R_{1\max}} e^{-\alpha \int_R^{R_{1\max}} dR} dl \quad (29)$$

This accounts for the different ranges for the same rain cell. It reduces to

$$k_{er} = \left(\frac{1 - e^{-\alpha \cdot 2 R_{1\max}}}{h_1 \alpha} \right) \cos(\theta) \quad (30)$$

which is the two-way attenuation of each rain cell (see Appendix I for derivation). Here $R_{1\max}$ is the range in the rain volume, and α from Table 1 is the attenuation coefficient in nepers/km, using the dB-to-nepers conversion. Substituting (29) in (27) will give the attenuated rain echo; similarly subtracting $2 \alpha_{dB} R_{1\max}$ from (23) will give the attenuated surface return, where α_{dB} is the attenuation dB/km. We substitute these attenuated returns in (24) to obtain a realistic estimate of the SCR; this is plotted in Fig. 6.

From Fig. 6 it is clear that for low rain rates the signal lies far below the clutter for angle of incidence of 30° . However, for higher angles, the clutter lies below the signal for moderate rain rates at low wind speeds.

5.0 SIGNAL-TO-NOISE-RATIO CALCULATIONS

To compute the minimum detectable rain rate it is necessary to compute the signal-to-noise ratio (SNR). But, before we compute the SNR, let us look at the SAR resolution in rain.

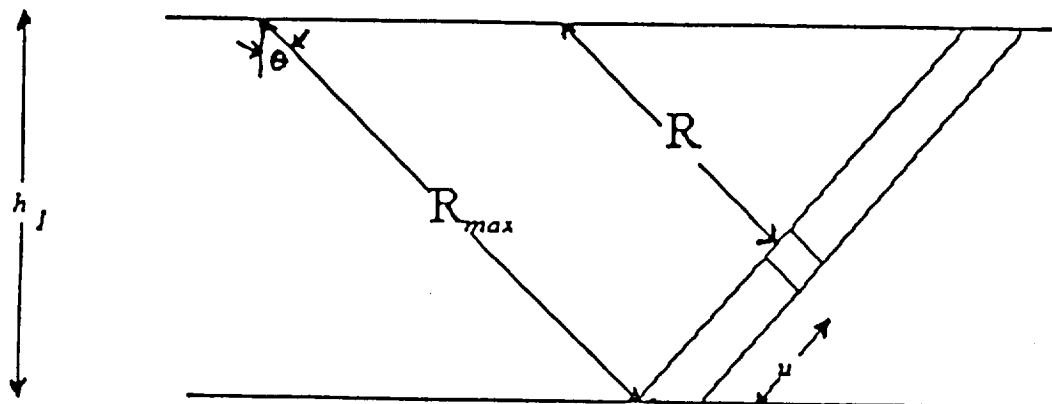
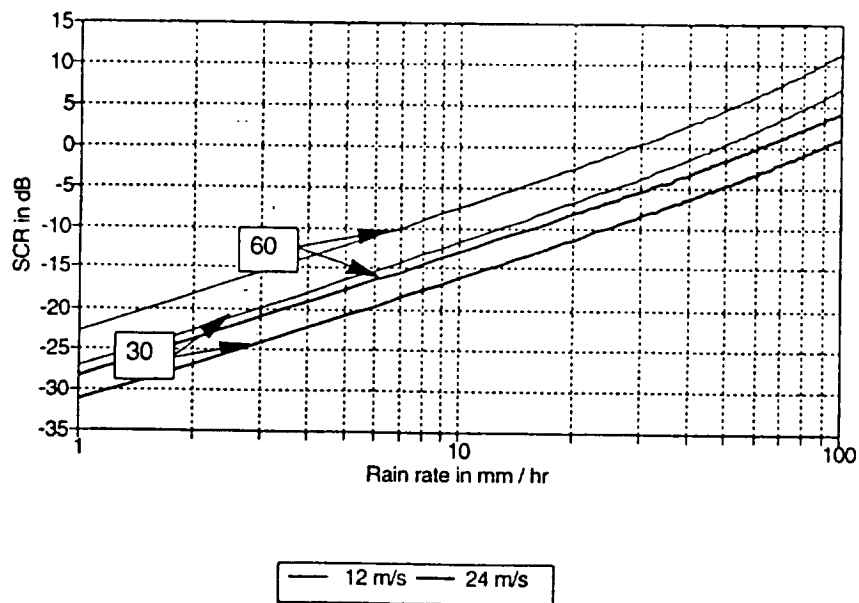


Fig.5 Different path lengths travelled through the rain by the signal from the same pulse volume

X-BAND



C-BAND

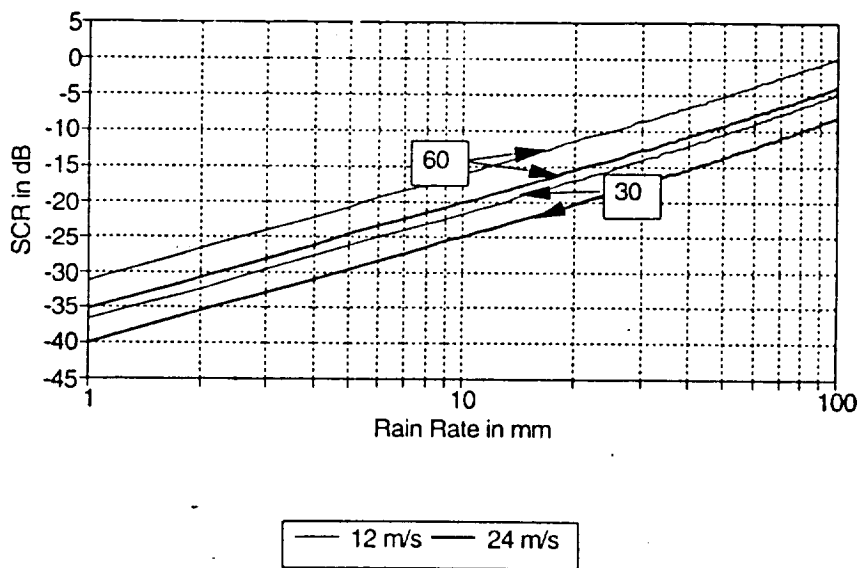


Fig.6 Plot of the X and C band SCR at 60° and 30° for cross wind speeds of 12 m/s and 24 m/s.

5.1 SAR RESOLUTION IN RAIN

SAR can use the full synthetic aperture only when the targets in the pulse volume are correlated, i.e., their phase positions remain essentially fixed. To find the maximum possible aperture that can be synthesized during T_a , the time during which the target is illuminated, let us consider the bandwidth between the isodops for a SAR.

$$B_{df} = \left(\frac{2 U r_{as}}{R \lambda} \right) \quad (31)$$

where U is the velocity of the platform, R is the range and the others have their usual meaning. The ratio between the synthetic-aperture length L_s and the time T_a to pass that length is simply the platform speed. Thus the maximum possible aperture that can be synthesized during the integration time T_a is

$$L_s = U T_a \quad (32)$$

Atlas and Moore (1987) show that a larger Doppler spread leads to shorter integration time. For a smaller synthetic aperture where the resolution element is large, it can be seen that the Doppler bandwidth is

$$B_{df}(precip) = 4 \frac{\sigma_{vs}}{\lambda} \quad (33)$$

From (31) we may write

$$r_{as} = 2 \sigma_{vs} \frac{R}{U} \quad (34)$$

and also

$$L_s = \lambda \frac{U}{4 \sigma_{vs}} \quad (35)$$

and the synthetic beam width is

$$\beta_s = 2 \frac{\sigma_{vs}}{R} \quad (36)$$

All this means that the synthetic beamwidth varies and is broadened in proportion to the Doppler spectral width of the target. Further, it means that the number of pulses that can be coherently integrated, the effective length of the synthetic aperture L_s , and the effective coherent-integration gain in the signal-to-noise ratio are inversely proportional to σ_{vs} .

This applies only when

$$\sigma_{vs} < \frac{\lambda U}{6 L_n} \quad (37)$$

where

U = the velocity of the spacecraft in m/s,

L_n = length of the along-track real aperture,

σ_{vs} = standard deviation of the Doppler velocity spectrum.

For X-SAR the standard deviation of the Doppler velocity (due to the wind turbulence, shear, etc.) must be less than 3.75 m/s for a three-fold improvement in the resolution for the SAR, compared to the RAR (i.e., for the synthetic beamwidth to be one-third of the real beamwidth).

This indicates that the effective beamwidth increases with increases in σ_{vs} , the spread of the target Doppler spectrum. Further, the integration gain decreases with σ_{vs} because the number of pulses that can be coherently integrated along track is proportional to the target coherency time and thus inversely proportional to σ_{vs} . Therefore, the echo power for the SAR is identical to that of a conventional radar using the same along-track beamwidth as the SAR. The only exception to this is when the Pulse Repetition Frequency (PRF) exceeds that given by $2 U/L_d$, where L_d is the length of the antenna. In this case the coherent gain increases in proportion to the oversampling ratio so that the SAR would have a larger (SNR) than a real-aperture radar.

5.2 THE SIGNAL-TO-NOISE RATIO

The basic radar equation for any target is

$$P_r = \frac{P_t G^2 \lambda^2 \sigma}{(4\pi)^3 R^4} \quad (38)$$

where the variables have their usual meaning.

If $\Sigma \sigma_i$ is the average total backscatter cross section of particles per unit volume (in m^2), the radar cross section may be expressed as

$$\sigma = V_m \Sigma \sigma_i \quad (39)$$

where V_m is the volume of the resolution cell. From Fig. 2 the volume of the radar beam for the off-nadir look angle may be expressed in terms of the horizontal and the vertical beam widths for a pulse of duration τ as

$$V_m = \frac{\pi}{4} \frac{\beta_h R h_1 c \tau}{2 \sin(\theta_{av})} \quad (40)$$

where h_1 is the thickness of the rain region. This volume corresponds to the cells of interest; i.e., the ideal rain cells discussed in the previous sections. The resulting equation is

$$P_r = \frac{P_t G^2 \lambda^2 \beta_h h_1 c \tau}{512 \pi^2 R^3 \sin(\theta_{av})} \Sigma_i \sigma_i \quad (41)$$

We can use Rayleigh approximation when the dropsize is $\ll \lambda$. This gives

$$\Sigma_i \sigma_i = \frac{\pi^5 \Sigma D^6}{\lambda^4} |k|^2 \quad (42)$$

where λ is in centimeters and k is a factor involving the complex permittivity.

Radar meteorologists have derived an empirical power law, the Z-R relationship, from the available data. That is,

$$Z = a R_r^{b_1} \quad (43)$$

where a and b_1 have been found to depend on the drops size distribution, rain type, rain rate, frequency, and region. The coefficients differ markedly at small and large values of R_r . However, with the exception of orographic rains, most differ only slightly at rainfall intensities between 20 and 200 mm/hr. Although it is clear that the Z-R relation is useful, the values of the coefficients a and b_1 have to be selected judiciously. A single Z-R relation for all types of rain cannot account for the variations for different types of rain. In relating (43) to (42) the relation $Z = \sum_i D_i^6$ is used.

Battan (1973) calculated the Z-R relation using the Mie scattering theory. Table 2 shows the various relationships for different wave lengths and drops size distributions. Clearly for a given wavelength, but for different rain rates, a takes drastically changing values. However, for modest and small rain rates, assuming the value of a to be around 300 and b_1 to be about 1.5 is reasonable. Here we use the relation

$$Z = 300 R_r^{1.5} \quad (44)$$

The radar equation in (41) does not include the various system losses, nor does it account for attenuation due to clouds, rain, the ice melting layer and the atmosphere. Additional factors added to (41) can account for this. The final form of the radar equation for meteorology (see 45) for non-nadir viewing angles can be obtained by substituting (43) and (46) in (41) with additional factors to account for losses

$$SNR = \frac{P_r}{K T B F} \frac{G^2 \lambda^3 \beta_h c \tau h l \eta L_s L_b^2}{512 \pi^2 R^3 \sin(\theta_{av})} 10^{-0.1(k_v)} \quad (45)$$

where

$$\eta = \frac{\pi^5 300 R^{1.5} k^2}{\lambda^4} 10^{-10} \quad (46)$$

G is the gain, B is the bandwidth, L_s is the system loss, L_b is the signal loss due to absorption by the ice melting layer, η is the rain reflectivity, K_{er} is the attenuation due to rain from (28), and F is the receiver noise figure. The other parameters have their usual meaning. The plots in the Fig. 7 are made from the data generated using (45) for different angles of incidence.

This SNR calculation is based on the assumption that the entire beam volume below the cloud top is rain-filled. If this is not true the SNR will decrease. The result of this is that the minimum detectable rain rate increases for fixed SNR. Studies show that a typical rain storm diameter for rain rates of 10 to 15 mm is 10 to 15 km (see Fig. 8). Thus, relative large storm diameters may be expected at lower rain rates, and the probability of partial beam filling along track is low. If however the cross-track beam is only partially filled we may consider the region 2 discussed earlier to a be special case of regions 1 and 3; i.e., (there will be at least a few ideal rain cells).

6.0 CONCLUSIONS

This preliminary study, involving many approximations, shows that, for non-nadir look angles, the signal returned due to the rain cell barely exceeds that returned from the ocean surface even for high rain rates.

The calculations and the plots are for ideal rain cells to get an idea of the bound, if not the actual magnitude, of the signal-to-clutter ratio. The plot (Fig. 6) for the signal-to-clutter ratio shows that the signal-to-clutter ratio lies above 0 dB for an angle of incidence 60° , $R_r > 20$ mm/hr for the upwind look direction, and $R_r > 10$ mm/hr for crosswind. At 30° the signal return barely lies above the clutter even for high rain rates. The minimum detectable rain rate, therefore,

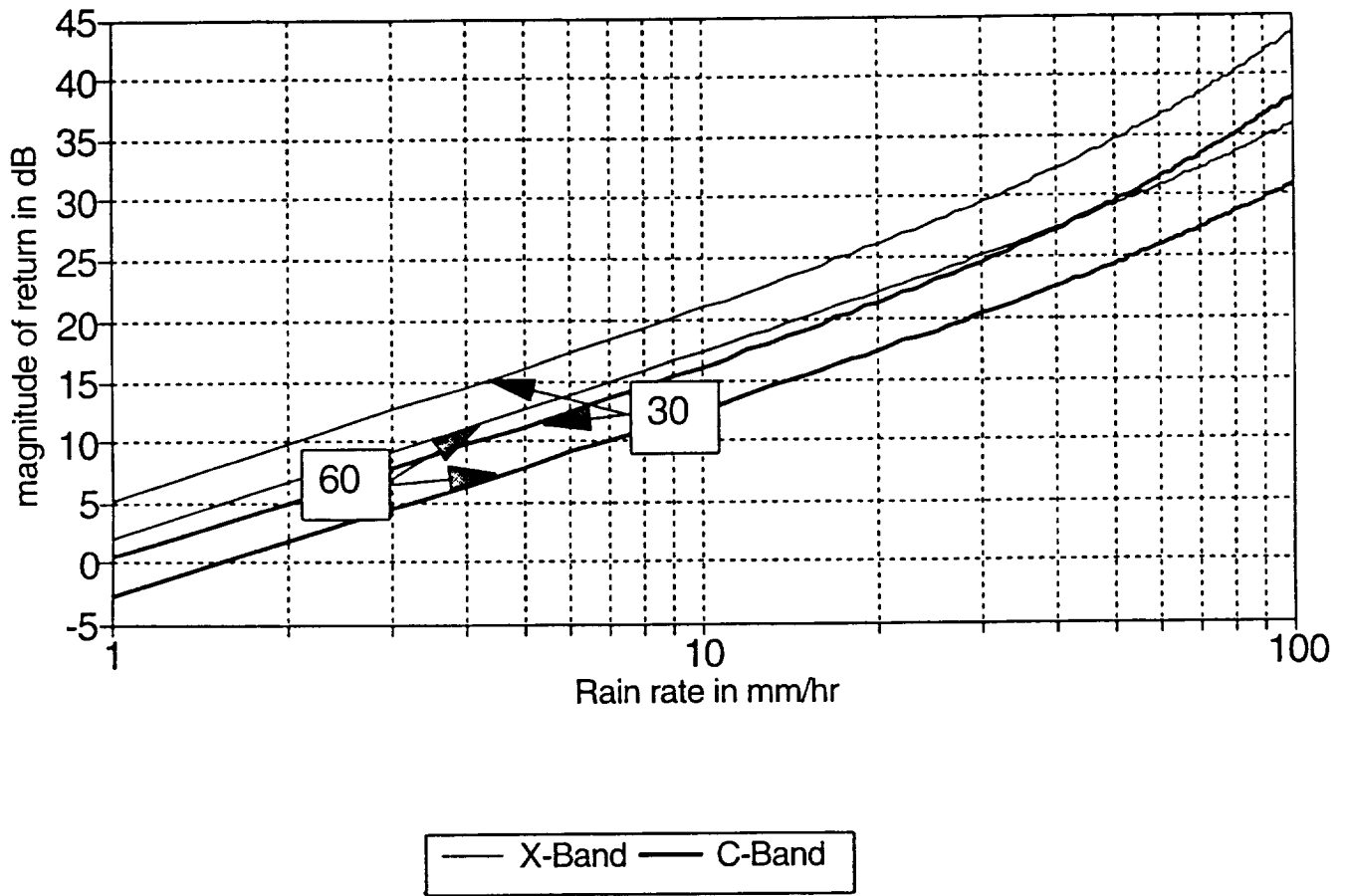


Fig.7 Plot of the SNR for X and C band at 30° and 60°.

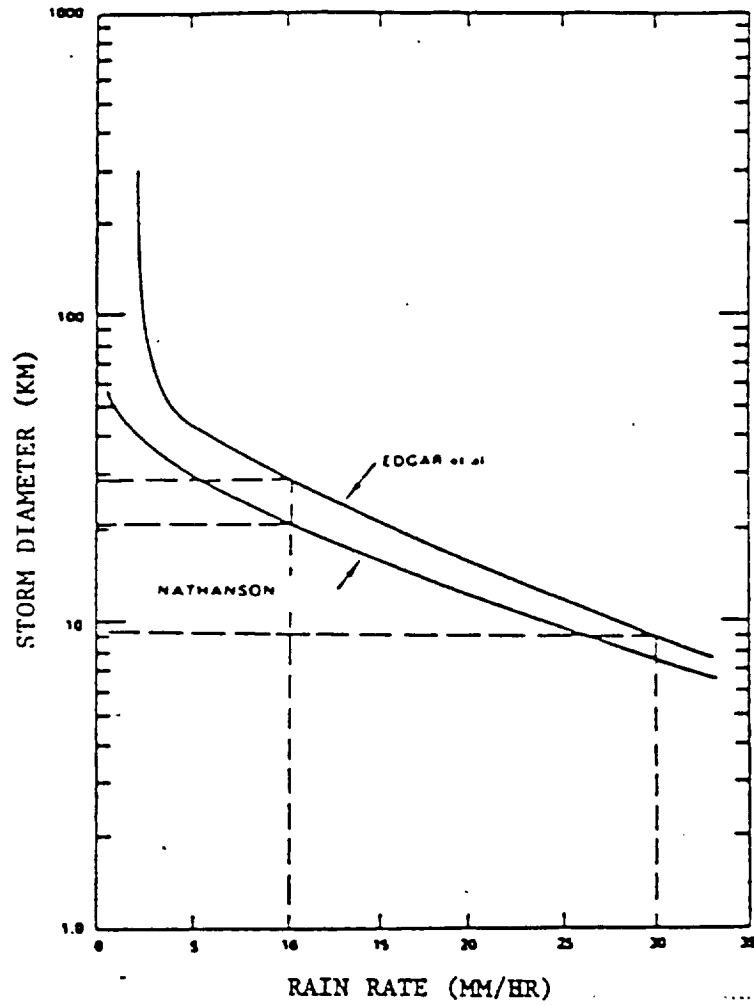


Fig.8 Plot of the storm diameter against rain rate (Goldhirsh and Rowland, 1982).

occurs at cross wind and lies well above 10 mm/hr, at high angles of incidence. Thus, off-vertical measurement of rain with X-SAR must be at high incidence angles.

If a situation arises where the wind on the surface is low and the rain rate is high, there is a possibility of over estimation of the actual rain rate because the modification of the backscatter due to impinging rain drops increases the clutter. Though the study addresses the problem of attenuation, it is seen that the attenuation is very small, around 2 dB at X band, even at very high rain rates of 100 mm/hr. The attenuation due to the clouds and the rain combined is less than 2 dB, which is of no great consequence for our calculations, in that the selected model for the surface is accurate to about 2 dB of the actual value. However we must accurately account for attenuation in actual measurements to avoid under estimation of the actual rain rate. The attenuation for various clouds may be looked up from the Table A in the Appendix I.

From all this we see that the limiting factor for the detection of modest rain rates at non-nadir look angles is not the lack of adequate signal-to-noise ratio, but the low signal-to-clutter ratio. Though the SNR is high, this high SNR is of no consequence because, though it may be possible to extract the signal from the noise, it will not be possible to determine the source of the signal return. This means that at small rain rates and off-nadir look angles the radar receives a signal that may be entirely due to the surface scatter, and it will be difficult to extract the rain rate using a conventional deconvolution algorithm. Thus, it may be concluded that the success of the experiment depends on finding high rain rates, accompanied by modest wind speeds, at locations where the angle of incidence is large or on using the nadir look angle. The study strongly recommends that measurements be made and data obtained at nadir look angles whenever possible. The next step in the investigation will involve addressing the SNR and SCR for the nadir look case.

Values of Parameters in the Relationships
 $\kappa_{pp} = \kappa_1 R_p^b$ (Logarithmic Model) and $\kappa_{pp} = \kappa_1 R_p$ (Linear Model)

Frequency (GHz)	Logarithmic model ^a				Linear model	
	κ_1		b		κ_1	Comments ^b
	V	H	V	H		
2.8	0.000459		0.954		—	(1)
7.5	0.00459		1.06		0.00481	(1)
9.4	0.0087		1.10		0.00932	(1)
11.0	0.012	0.014	1.23	1.24	—	(2)
16.0	0.0374		1.10	1.24	0.0403	(1)
18.0	0.053	0.061	1.07	1.10	—	(2)
24.0	0.10	0.11	1.03	1.06	—	(2)
30.0	0.17	0.19	0.98	1.00	—	(2)
34.9	0.225		1.05		0.234	(1)
40.0	0.31	0.38	0.91	0.93	—	(2)
60.0	0.63	0.71	0.81	0.82	—	(2)
69.7	0.729		0.893		—	(1)
80.0	0.86	0.93	0.76	0.77	—	(2)
100.0	1.06	1.15	0.73	0.73	—	(2)

^aThe symbols V and H refer to vertical and horizontal polarizations.

^b(1) Computed for spherical particles by Crane (1971); (2) computed for oblate spheroidal drops, reported by Harden et al. (1978).

Table.1 The attenuation coefficients at various frequencies may be picked off from here to be used in the relation discussed (Ulaby, et al. 1981).

Wavelength (Cm)	R Interval (Mm/Hr)	M-P (0°C)	Z ₀ (Mm ³ /M ³) Gunn and East (18°C)	Mueller and Jones (0°C)
0.62	0-5	240R ^{1.1}	450R
	5-20	345R ^{0.9}
	20-100	540R ^{0.75}
0.86	0-5	350R ^{1.25}	950R
	5-20	450R ^{1.15}
	20-100	780R ^{0.95}
1.24	0-5	356R ^{1.3}	1280R
	5-20	460R ^{1.25}
	20-100	820R ^{1.15}
1.87	0-20	330R ^{1.35}	1150R
	20-50	500R ^{1.2}
	50-100	750R ^{1.1}
3.21	275R ^{1.35}	310R ^{1.35}	890R
4.67	280R ^{1.45}	860R
5.5	280R ^{1.45}	860R
5.7	210R ^{1.6}
10	295R ^{1.45}	210R ^{1.6}	810R

Source: Wesler and Atlas 1963.

Table.2 Z-R relation calculated using mie scattering (Battan,1973).

REFERENCES

- Atlas, D. and R.K. Moore, "The measurement of precipitation with the synthetic aperture radar," *Journal of Atmospheric and Oceanic Technology*, vol.4, pp.368-376, 1987.
- Battan, L.J., *Radar Observation of the Atmosphere*, University of Chicago Press; Chicago, 1973.
- Blivens, L.F. and G.Norcross, "Effects of rainfall on scatterometer derived wind speeds," *IGARSS'88 Digest*, vol I, pp.565-567, 1988.
- Chan, H.L. and A.K. Fung, "A theory of sea scatter at large incidence angles," *Journal of Geophysical Res.*, vol. 82, pp.3429-3444, 1977.
- Goldhirsh, J., and J.R. Rowland, "A tutorial assessment of atmospheric height uncertainties for high-precision satellite altimeter missions to monitor ocean currents," *IEEE Trans. Geo. and Rem. Sens.*, vol. GE-20, pp.418-434, 1982.
- Goldhirsh, J., "Analysis of algorithms for retrieval of rain-rate profiles from a space borne dual wavelength radar," *IEEE Trans. on Geo. and Rem. Sensing*, vol. 26, no. 2, pp.98-114, 1988.
- Hansen, J.P., "Rain backscatter test dispel old theories," *Microwaves and RF*, vol. 25, pp.97-102, June 1986.
- Jones, W.L., L.C Schroeder, and J.L. Mitchell, "Aircraft measurement of the anisotropic scattering signature over the ocean for the JONSWAP and 1976 east coast missions," NASA TMX 28646, 1978.
- Moore, R.K., Y.S. Yu, A.K. Fung, D. Kaneko, G.J. Dome, and R.E. Werp "Preliminary study of rain effects on rain scattering from water surfaces," *IEEE J. Ocean. Engr.*, vol. OE-4, pp.31-31, 1979.

- Schroeder, L.C., P.R. Send, J.L. Mitchell, and L.W Jones, "AAFE RADSCAT 13.9 G-Hz measurements and analysis: Wind-speed signature of the ocean," *IEEE J. Ocean. Engr.*, vol OE-10 no.4, pp.346-357, 1985.
- Soofi.K, "Clutter model for land, forest, snow, sea ice and ocean," RSL Tech. Report 2923-2, 1978.
- Stuart, M. A, "Radar sensitivity and antenna scan pattern study for a satellite based radar wind sounder," MS thesis, University of Kansas, 1992.
- Ulaby, F.T., R.K. Moore, and A.K. Fung, *Microwave Remote Sensing*, Vol III Artech House:Norwood, MA, 1986.

APPENDIX - 1

ANALYSIS OF EFFECT OF RANGE VARIATION ON ATTENUATION

The rain return involves

$$\sigma_v e^{-\int_R^{R_{max}} \alpha dR} V_m \quad (\text{a})$$

where V_m is the volume and σ_v is the scattering coefficient and α is the attenuation coefficient in nepers/km. Since the range changes along the same rain cell (see Fig. 5) it is necessary to integrate the attenuation over these ranges. We can write (a) as

$$\sigma_v V_{eff} = I_a I_R \sigma_v \int e^{-\alpha \int_R^{R_{max}} dR} du \quad (\text{b})$$

From Fig. 5

$$\frac{R}{R_{max}} = \frac{(u_{max} - u)}{u_{max}} \quad (\text{c})$$

which may be written as

$$R = \frac{(u_{max} - u)}{u_{max}} R_{max} \quad (\text{d})$$

Now substituting $R_{max} = h_1 / \cos\theta$ and $u_{max} = h_1 / \sin\theta$ in (c) we have

$$R = \left(1 - \frac{u \sin\theta}{h_1}\right) \frac{h_1}{\cos\theta} \quad (\text{e})$$

and substituting in (e) in (b) we have

$$\sigma_v V_{eff} = I_a I_R \sigma_v e^{-\frac{\alpha h_1}{\cos\theta} \int_0^{u_{max}} e^{\alpha \tan\theta} du} \quad (\text{f})$$

solving the integral, and making the substitution $u_{max} \tan\theta = h_1 / \cos\theta$ we have

$$\sigma_v V_{eff} = \frac{r_a r_R \sigma_v}{\alpha \tan\theta} (1 - e^{-\frac{\alpha h l}{\cos\theta}}) \quad (\mathbf{g})$$

Now, if we write $V_{eff} = r_a r_R L_{eff}$ and compare both sides, we see that

$$L_{eff} = \frac{1 - e^{-\alpha R_{max}}}{\alpha \tan\theta} \quad (\mathbf{h})$$

The equation is used in the report to account for the variation of the attenuation in the same rain cell. This works only for α large enough that L is not limited by the beamwidth. If L be the actual length of the cell we may write $L_{eff} = f_{ah} L$, where f_{ah} is the attenuation factor.

Note: k_a and k_s are subject to the Rayleigh Criteria

Cloud Layer	Cloud Name	10 GHz		
		k_a	k_s	k_e
10-1(w)	AltoCumulus	-0.03	0.00	-0.03
14-1(w)	AltoCumulus	-0.03	0.00	-0.03
20-1(w)	Low-Lying Stratus	-0.05	0.00	-0.05
20-2(w)	Low-Lying Stratus	-0.05	0.00	-0.05
21-1C(w)	Drizzle, 0.2 mm/hr	-0.19	0.00	-0.19
21-1B(w)		-0.37	0.00	-0.37
21-2D(w)	Steady Rain, 3 mm/hr	-0.19	0.00	-0.19
21-2C(w)		-0.37	0.00	-0.37
21-2B(w)		-0.19	0.00	-0.19
21-3D(w)	Steady Rain, 15 mm/hr	-0.37	0.00	-0.37
21-3C(w)		-0.56	0.00	-0.56
21-3B(w)		-0.37	0.00	-0.37
22-1(w)	StratoCumulus	-0.05	0.00	-0.05
22-2(w)	StratoCumulus	-0.05	0.00	-0.05
25-1C(w)	Fair Weather Cumulus	-0.09	0.00	-0.09
25-1B(w)		-0.19	0.00	-0.19
25-1A(w)		-0.09	0.00	-0.09
25-2C(w)	Cumulus, 2.4 mm/hr	-0.37	-0.01	-0.38
25-2B(w)		-0.19	0.00	-0.19
25-3C(w)	Cumulus, 12 mm/hr	-0.74	0.00	-0.74
25-3B(w)		-0.37	-0.01	-0.38
25-4E(w)	Cumulus Congestus	-0.09	0.00	-0.09
25-4D(w)		-0.19	0.00	-0.19
25-4C(w)		-0.15	0.00	-0.15
25-4B(w)		-0.09	0.00	-0.09
25-4A(w)		-0.06	0.00	-0.06
26-1E(w)	Cumulonimbus, 150 mm/hr	-0.56	0.00	-0.56
26-1D(w)		-0.74	0.00	-0.74
26-1C(w)		-1.48	0.00	-1.49
26-1B(w)		-1.30	-0.02	-1.32

Table. A Absorption and extinction 2 way coefficients based on the Deirmendjian model(all values in dB/km, M.A Stuart,1992)

Parameters for SIR-C/X-SAR sensor used to evaluate the SNR and SCR

Parameters	L-band	C-band	X-band
-Frequency (GHz)	1.25	5.3	9.7
-Wavelength (cm)	23.5	5.7	3.1
Polarization	HH,VV,HV,VH	HH,VV,HV,VH	VV
Tran. Peak Power (KW)	3.8	2.05	3.0
-Pulse Duration (μ s)	33	33	40
Pulse Rep. Frequency (KHz)	1.2-1.8	1.2-1.8	1.2-1.8
Bandwidth (MHz)	10-20	10-20	9.5
-Antenna Size (m)	12 \times 2.9	12 \times 0.7	12.1 \times 0.3
Antenna Beamwidths (deg)	1.15 \times 4.74	0.27 \times 4.63	0.15 \times 5.92
-Antenna Gain (dB)	37	43	42
Antenna Size-lobe Level (dB)	-50	-50	-50
-Sys. Noise Temperature ($^{\circ}$ K)	603	739	992
-System Loss (dB)	0	0	-1.8
Processing Loss (dB)	-3	-3	-3